

in the Solar System²⁶ and the equations of precession for the Earth²⁷ over 100 Myr using several different values of ξ_i . We assumed, somewhat arbitrarily, that the Earth's obliquity was 55° at 600 Myr ago—the age of the youngest low-latitude glacial deposits^{3–5}. Williams suggested that the obliquity must originally have been >54° because this is the critical latitude above which the poles receive more annually averaged insolation than does the Equator. However, ice sheets are more sensitive to changes in seasonal insolation extremes than to annually averaged insolation, so the Earth's obliquity during Precambrian times need not actually have been this high. Figure 3 shows that under extreme polar ice loading, the Earth's obliquity could have been reduced to within 3° of its present value by 500 Myr ago if $\xi_i = 230^\circ$. (A phase lag near 0° yields a comparable rate of drift in the same direction (Fig. 2)). This result is in good agreement with the geological data referenced earlier¹¹.

Support for the hypothesis that the Earth's obliquity has decreased comes from analysing the orbit of the Moon. The lunar orbit is presently inclined at ~5° to the ecliptic plane. Backwards integrations by Goldreich²⁸ and others²⁹ have predicted that the lunar orbit was inclined by at least 10° to the Earth's equatorial plane when it formed. This result is in apparent conflict with the widely accepted giant-impact theory of lunar origin, in which the Moon accretes from an impact-generated debris disk aligned with the Earth's Equator³⁰. Had the Moon formed in the Earth's equatorial plane, as predicted, its orbit should have aligned itself with the ecliptic plane as the Moon receded from the Earth³¹. The present 5° lunar inclination with respect to the ecliptic plane implies that either the Moon was never in the equatorial plane (that is, that the giant-impact model is wrong) or that it was perturbed away from the equatorial plane early in its history, perhaps as a result of spin-orbit resonances encountered by the Earth and Moon when they were much closer^{31,32}. (The Moon's orbit might also have been inclined by a giant impact, but the extreme size of the necessary impactor²³ (>1,100 km) makes such an event unlikely.)

Alternatively, the lunar orbit may have tilted away from the ecliptic plane more recently in gravitational response to the secular downward drift of the Earth's obliquity around ~600 Myr ago. At present, the Earth's mean obliquity is slowly increasing as a result of tidal interactions with the Moon²⁸. The lunar inclination is decreasing at the same time, so the angular momentum of the Earth–Moon system is approximately conserved. Momentum conservation between the Earth's spin and the Moon's orbit may be approximately written $\sin(\Theta_e/2) = -(L_m/L_\oplus) \sin(\Theta_i/2)$, where $L_\oplus = C\omega$ is the spin angular momentum of the Earth, $L_m = M_m(GM_\oplus)^{1/2} a_m^{1/2}$ is the orbital angular momentum of the Moon, and Θ_e and Θ_i are the angular change to the Earth's obliquity and lunar inclination, respectively, C is one of Earth's principal inertia moments, defined in legend to Fig. 1, and M_m and M_\oplus are the masses of the Moon and the Earth, respectively.

For the late Proterozoic, the distance to the Moon, $a_m \approx 57$ Earth radii, and the rotational velocity of the Earth, $\omega \approx 2\pi/(21 \text{ hours})$ (ref. 33). If we assume that the lunar inclination was originally zero, and that the change that occurred as a result of climate friction was $\Theta_i = +6^\circ$ (allowing for a subsequent 1° reduction, to 5°, as a result of tidal friction), then the required change to the Earth's obliquity is $\Theta_e = -25.4^\circ$. This implies that the Earth's obliquity may have been $23.5^\circ + 25.4^\circ \approx 49^\circ$ for much of the Precambrian period, which is only slightly less than the 54° obliquity suggested by Williams. Given the uncertainty in the actual obliquity that would be required to cause low-latitude glaciation, we believe that the information obtained from the lunar orbit provides additional support for the idea that the low-latitude glaciations in Precambrian times were a consequence of high planetary obliquity. □

Received 12 January; accepted 10 September 1998.

- Evans, D. A., Beukes, N. J. & Kirschvink, J. L. Low-latitude glaciation in the Palaeoproterozoic era. *Nature* **386**, 262–266 (1997).
- Williams, G. E., Schmidt, P. W. Paleomagnetism of the Palaeoproterozoic Gowganda and Lorrain formations, Ontario: low paleolatitude for Huronian glaciation. *Earth Planet. Sci. Lett.* **153**, 157–169 (1997).

- Frakes, L. A. *Climates Throughout Geologic Time* (Elsevier, Amsterdam, 1979).
- Embleton, B. J. & Williams, G. E. Low paleolatitude of deposition for late Precambrian periglacial varvites in South Australia: implications for palaeoclimatology. *Earth Planet. Sci. Lett.* **79**, 419–430 (1986).
- Zhang, H. & Zhang, W. Palaeomagnetic data, late Precambrian magnetostratigraphy, and tectonic evolution of eastern China. *Precamb. Res.* **29**, 65–75 (1985).
- Schmidt, P. W. & Williams, G. E. The Neoproterozoic climatic paradox: Equatorial paleolatitude for Marinoan glaciation near sea level in South Australia. *Earth Planet. Sci. Lett.* **134**, 107–124 (1995).
- Park, J. K. Paleomagnetic evidence for low-latitude glaciation during deposition of the Neoproterozoic Rapitan Group, Mackenzie Mountains, N.W.T., Canada. *Can. J. Earth Sci.* **34**, 34–49 (1997).
- Hoffman, P. F., Kaufman, A. J., Halverson, G. P. & Schrag, D. P. A Neoproterozoic snowball Earth. *Science* **281**, 1342–1346 (1998).
- Meert, J. G. & Van der Voo, R. The Neoproterozoic (1000–540 Ma) glacial intervals: No more snowball earth? *Earth Planet. Sci. Lett.* **123**, 1–13 (1994).
- Williams, G. E., Schmidt, P. W., Embleton, B. J., Meert, J. G. & Van der Voo, R. The Neoproterozoic (1000–540 Ma) glacial intervals; no more snowball earth?; discussion and reply. *Earth Planet. Sci. Lett.* **131**, 115–125 (1995).
- Williams, G. E. History of the Earth's obliquity. *Earth Sci. Rev.* **34**, 1–45 (1993).
- Ward, W. R. Climatic variations on Mars: I. Astronomical theory of insolation. *J. Geophys. Res.* **79**, 3375–3386 (1974).
- Rubincam, D. P. The obliquity of Mars and "climate friction". *J. Geophys. Res.* **98**, 10827–10832 (1993).
- Crowley, T. J. & Baum, S. K. Effect of decreased solar luminosity on Late Precambrian ice extent. *J. Geophys. Res.* **98**, 16723–16732 (1993).
- Caldeira, K. & Kasting, J. F. Susceptibility of the early Earth to irreversible glaciation caused by carbon dioxide clouds. *Nature* **359**, 226–228 (1992).
- Vanyo, J. P. & Awramik, S. M. Length of day and obliquity of the ecliptic 850 Ma ago—preliminary results of a stromatolite growth model. *Geophys. Res. Lett.* **9**, 1125–1128 (1982).
- Awramik, S. M. & Vanyo, J. P. Heliotropism in modern stromatolites. *Science* **231**, 1279–1281 (1986).
- Rochester, M. G. The secular decrease of obliquity due to dissipative core-mantle coupling. *Geophys. J. R. Astron. Soc.* **46**, 109–126 (1976).
- Bills, B. G. Obliquity-oblateness feedback: Are climatically sensitive values of obliquity dynamically unstable? *Geophys. Res. Lett.* **21**, 177–180 (1994).
- Rubincam, D. P. Has climate changed Earth's tilt? *Paleoceanography* **10**, 365–372 (1995).
- Peltier, W. R. & Jiang, X. Precession constant of the Earth: Variations through the ice-age. *Geophys. Res. Lett.* **21**, 2299–2302 (1994).
- Ito, T., Masuda, K., Hamano, Y. & Matsui, T. Climate friction: A possible cause for secular drift of Earth's obliquity. *J. Geophys. Res.* **100**, 15147–15161 (1995).
- Williams, D. M. *The Stability of Habitable Planetary Environments*. Thesis. Pennsylvania State Univ. (1998).
- Hecht, J. & Scotese, C. R. *Ages of the Earth* (MacMillan, New York, 1997).
- Imbrie, J. et al. On the structure and origin of major glaciation cycles: 1. linear responses to Milankovitch forcing. *Paleoceanography* **7**, 701–738 (1992).
- Levison, H. F. & Duncan, M. J. The long-term dynamical behavior of short-period comets. *Icarus* **108**, 18–36 (1994).
- Laskar, J., Joutel, F. & Robutel, P. Orbital, precessional, and insolation quantities for the Earth from –20 Myr to +10 Myr. *Astron. Astrophys.* **270**, 522–533 (1993).
- Goldreich, P. History of the lunar orbit. *Rev. Geophys.* **4**, 411–439 (1966).
- Touma, J. & Wisdom, J. Evolution of the Earth–Moon system. *Astron. J.* **108**, 1943–1961 (1994).
- Ida, S., Canup, R. M. & Stewart, G. R. Lunar accretion from an impact-generated disk. *Nature* **389**, 353–357 (1997).
- Rubincam, D. P. Tidal friction and the early history of the Moon's orbit. *J. Geophys. Res.* **80**, 1537–1548 (1975).
- Touma, J. & Wisdom, J. Resonances in the early evolution of the Earth–Moon system. *Astron. J.* **115**, 1653–1663 (1998).
- Walker, J. C. G. & Zahnle, K. J. Lunar nodal tide and the distance to the Moon during the Precambrian. *Nature* **320**, 600–602 (1986).
- Peltier, W. R. Ice age paleotopography. *Science* **265**, 195–201 (1994).

Acknowledgements. We thank H. Levison and M. Duncan for the orbital integration code (SWIFT) and J. Laskar for the code used to integrate the precession equations. We also acknowledge discussions with J. Melosh and R. Canup concerning the lunar inclination. D.M.W. was supported by a NASA graduate student research fellowship awarded in 1995, and J.F.K. was supported by the NASA Exobiology Program.

Correspondence and requests for materials should be addressed to D.M.W. (e-mail: dmw145@psu.edu).

Asymmetric sea-floor spreading caused by ridge–plume interactions

R. Dietmar Müller*, Walter R. Roest† & Jean-Yves Royer‡

* The University of Sydney, School of Geosciences, Building F05, NSW 2006, Australia

† Geological Survey of Canada, 615 Booth Street, Ottawa, ON, K1A 0E9 Canada

‡ Unité Mixte de Recherche 6526, Géosciences Azur, Quai de la Darse – BP 48, 06235 Villefranche sur mer, Cedex, France

Crustal accretion at mid-ocean ridges is generally modelled as a symmetric process. Regional analyses, however, often show either small-scale asymmetries, which vary rapidly between individual spreading corridors, or large-scale asymmetries represented by consistent excess accretion on one of the two separating plates over geological time spans^{1–6}. In neither case is the origin of the

asymmetry well understood. Here we present a comprehensive analysis of the asymmetry of crustal accretion over the past 83 Myr based on a set of self-consistent digital isochrons⁷ and models of absolute plate motion^{8,9}. We find that deficits in crustal accretion occur mainly on ridge flanks overlying one or several hotspots. We therefore propose that asymmetric accretion is caused by ridge propagation towards mantle plumes or minor

ridge jumps sustained by asthenospheric flow^{10,11} between ridges and plumes. Quantifying the asymmetry of crustal accretion provides a complementary approach to that based on geochemical¹² and other geophysical data^{13,14} in helping to unravel how mantle plumes and mid-ocean ridges are linked through mantle convection processes.

To analyse global spreading asymmetries, we constructed a grid of

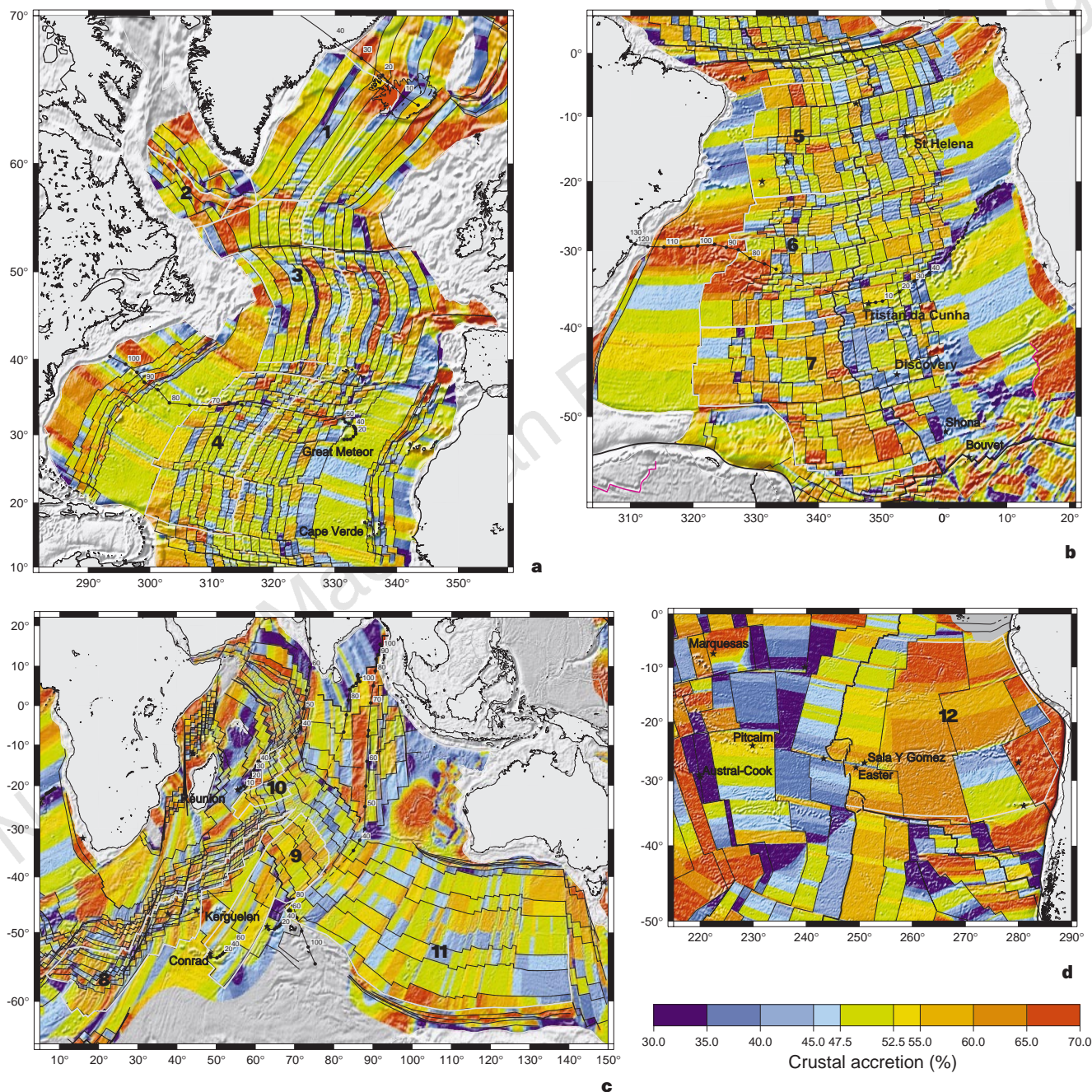


Figure 1 Crustal accretion rates of conjugate plates in four areas, illuminated by marine gravity anomalies²⁷. **a**, The North Atlantic; **b**, the South Atlantic; **c**, the Indian Ocean; and **d**, the South Pacific Ocean. The isochrons shown are 5 (10.9 Myr ago), 6 (20.1 Myr ago), 13 (33.1 Myr), 18 (40.1 Myr), 21 (47.9 Myr), 25 (55.9 Myr), 31 (67.7 Myr), 34 (83.5 Myr), M0, M4, M10, M16, M21 and M25 (ref. 7). Isochrons in the southwest Pacific are based on Munschy *et al.*²⁸. Areas for which we analysed the asymmetry of crustal accretion through time are outlined by grey polygons and numbered from 1 to 12. Also shown are synthetic tracks of hotspots crossing the ridge (from ref. 8); labels are in million of years (see ref. 29 for a discussion on model accuracy). The gaps in hotspot tracks created by ridge

crossings are dashed. Hotspots that have been close to a ridge for long geological time periods may simultaneously produce hotspot tracks on two plates (for example, Kerguelen, Tristan). Present-day locations of hotspots are shown as stars, and the main hotspots are labelled. Active plate boundaries are shown as bold black lines, whereas extinct ridges are coloured magenta. Continental margins are light grey, and areas of insufficient data coverage are dark grey; AAD indicates Australia–Antarctic discordance. Asymmetries off western Australia represent deviations from spreading rates based on best-fit half-stage poles, as conjugate Indian Ocean floor is subducted.

crustal accretion rates using the global age data set of Müller *et al.*⁷ (Fig. 1). Resolution is limited by the isochron spacing and the grid node interval of 0.1°. We assessed the internal consistency by extracting the spreading asymmetry for conjugate plate pairs from two selected areas of equal time range for Africa–South America (area 5, Fig. 1b) and Australia–Antarctica (area 11, Fig. 1c), and tested whether the percentages of crustal accretion add up to 100%. The mean error for these two plate pairs is $0.23 \pm 1.8\%$. However, errors in cumulative plate accretion for the same plate pairs are much smaller, that is, 0.075% for area 5 and 0.005% for area 11.

At relatively small scales, asymmetries in crustal accretion vary between individual spreading corridors and through time without clear trends, and independently of the presence of ridge propagators (Fig. 1). This is in accordance with patterns of spreading asymmetry found on a local scale on the Mid-Atlantic Ridge^{3,5,6}. Such short-term asymmetries in crustal accretion may be caused by long-lived asymmetries in small-scale convection under the ridge¹⁵, by intra-segment ridge propagation³ or variations in melt supply⁵. On the timescales that we can resolve (stage durations of ~6–14 Myr) there is no correlation between the short-term asymmetry of spreading and half-spreading rates, or the migration of the ridge relative to the mantle.

In order to analyse short- versus long-term spreading asymmetries (Fig. 2), we calculated the rates of mid-ocean-ridge migration

relative to the mantle, parallel to the spreading direction, using absolute plate motion models^{8,9} (Fig. 3). Small-scale, short-term asymmetries do not correlate with spreading rates or absolute ridge migration rates within the resolution of our data. However, Figs 2 and 4 clearly show cumulative, long-term asymmetries. We first evaluate their correlation with ridge migration rates. The South Atlantic ridge (areas 5, 6, 7) exhibits the slowest rates of ridge migration of the ridges considered here (2.4–3.9 mm yr⁻¹). Rates of excess accretion have been consistently high on South America (2.4–4.1%). The ridges in the North Atlantic (areas 1, 2, 3, 4) all migrated with average rates of 16–19 mm yr⁻¹, and show small totals of excess accretion between 0.6% and 0.7% on the leading plate. In contrast, the southwest (area 8) and western southeast Indian (area 9) ridges migrated northwards at average rates of ~16 and 49 mm yr⁻¹, but show excess accretion on the trailing plate (that is, Antarctica) of 3.1% and 1.7%, respectively. The central Indian ridge (area 10) migrated northeastwards about as fast as the western southeast Indian ridge, but shows a ‘flip’ in excess accretion from the leading plate to the trailing plate at chron 13 (33.1 Myr ago), resulting in negligible cumulative asymmetry (0.5%). On the eastern southeast Indian ridge (area 11) the leading Australian flank shows excess accretion on average for the past 35 Myr, while the ridge has been moving north at rapid rates averaging ~40 mm yr⁻¹

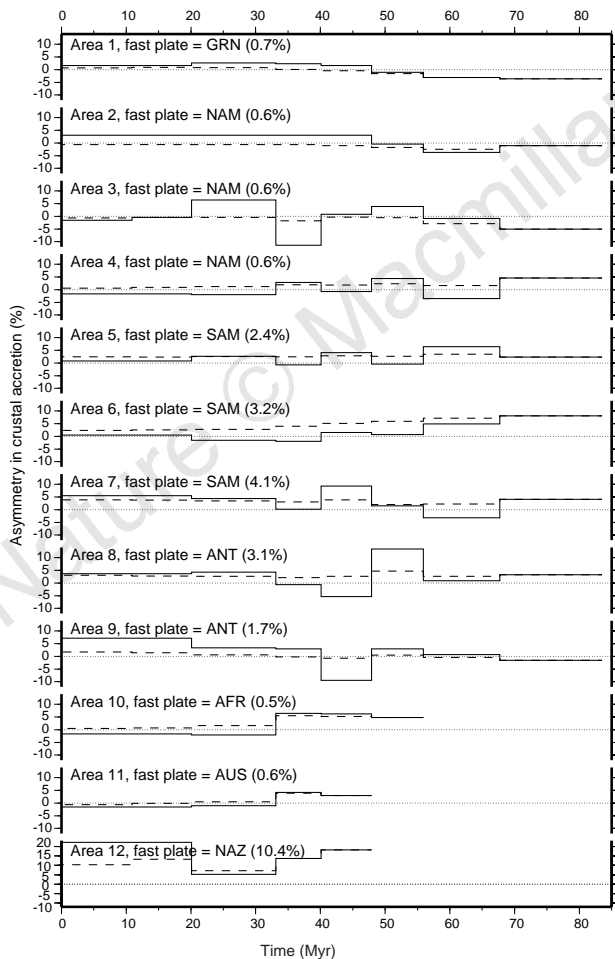


Figure 2 Spreading asymmetry by stage (continuous lines) versus time for areas marked in Fig. 1. The total, cumulative difference in accreted area for each plate pair is given in per cent (dashed lines). For each plate pair, the two graphs are identical for the first stage (83.5–67.7 Myr), and then diverge to express fluctuations in accretion asymmetry through time versus cumulative trends. The zero-age value of the cumulative curve distinguishes ‘fast plates’ (cumulative excess accretion) from ‘slow plates’. GRN, Greenland; NAM, North America; SAM, South America; ANT, Antarctica; AFR, Africa; AUS, Australia; NAZ, Nazca.

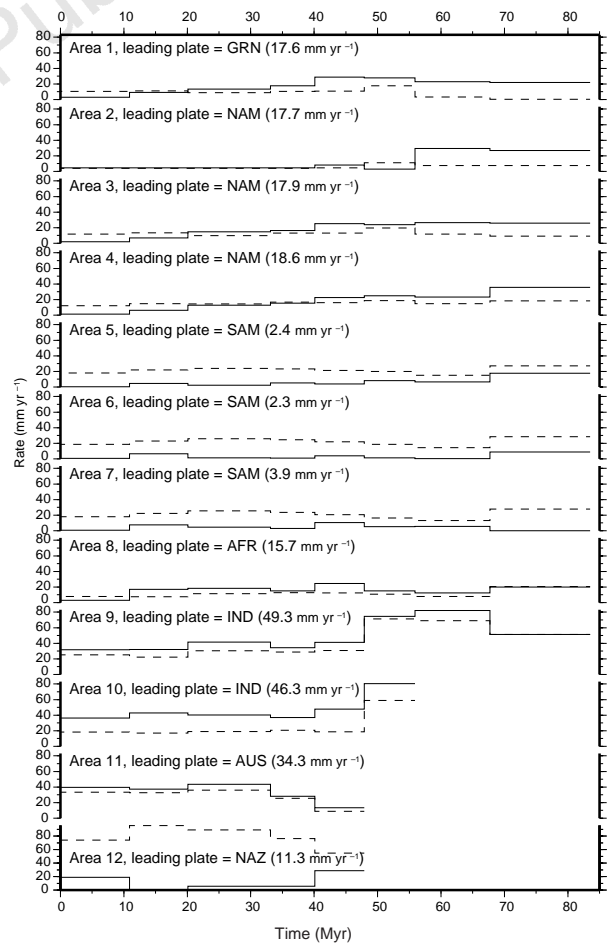


Figure 3 Rate of the ridge-normal component of the migration of mid-ocean ridges relative to the mantle by stage versus time (solid lines). Rates are computed for points roughly in the middle of the mid-ocean-ridge segments analysed (Fig. 1). Half-spreading rates are shown as dashed lines. The average, cumulative ridge migration rate is given for the leading plates, that is, the plates which move faster relative to the mantle than their conjugates. IND, India; other abbreviations as in Fig. 2.

since 33 Myr ago. On the East Pacific Rise (area 12, Fig. 1d) ridge migration is quite slow (11.3 mm yr^{-1}) despite fast spreading rates (Fig. 3). Here we find excess accretion on the leading Nazca plate (10.4% since 40 Myr ago).

Thus, contrary to the model suggested by Stein *et al.*¹⁶, there appears to be no correlation between long-term spreading asymmetry and migration of the spreading ridge over a fixed or slowly moving mantle. Based on a fluid mechanical flow model, Stein *et al.*¹⁶ suggested that trailing plates should accrete faster. However, Sleep¹⁷ and Fujita and Sleep¹⁸ showed that the fast side of a spreading ridge is hotter and weaker, and therefore more susceptible to dyke intrusion. This acts as a stabilizing mechanism, and may help explain why ridge migration does not necessarily result in long-term asymmetries. Only the spreading ridge between India and the trailing, Antarctic, ridge flank shows consistent excess accretion on the trailing plate as implied by Stein *et al.*¹⁶. This ridge also moved at relatively high rates of $30\text{--}80 \text{ mm yr}^{-1}$ relative to the mantle since chron 34 (83 Myr ago) (Fig. 3), suggesting a minimum 'absolute' ridge migration speed for Stein *et al.*'s¹⁶ mechanism to have an effect on the asymmetry of spreading.

A connection between asymmetries in crustal accretion and in asymmetric depth-age behaviour as suggested by Hayes⁴ is not evident. For instance, in the southern South Atlantic (area 7) there is excess accretion on the anomalously deep¹⁹ South American ridge flank, whereas in the western southeast Indian Ocean (area 9) pronounced excess accretion occurs on the anomalously shallow²⁰ Antarctic ridge flank. Where plate-wide asymmetries are observed, they do not occur in all spreading corridors (Fig. 1). Stein *et al.*¹⁶ noted that if hotspot-ridge asthenospheric flow is relatively fast compared to ridge migration speed, then the latter alone will not predict spreading asymmetry.

The generation of long-term asymmetries requires dyke intrusion to consistently move towards the slower-spreading flank, which is cooler in the absence of hotspots. To investigate the effect of hotspots on spreading asymmetries, we show synthetic tracks of

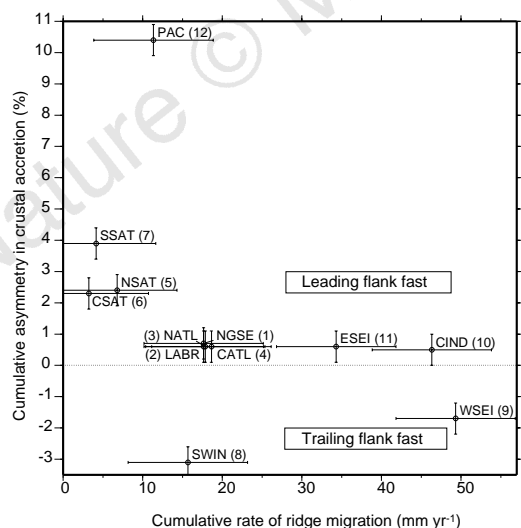


Figure 4 Cumulative rate of ridge migration versus spreading asymmetry and estimated errors. Data are given for areas marked in Fig. 1 averaged for time periods shown in Figs 2 and 3. Most leading ridge flanks are fast, because the conjugate trailing flanks are underlain by one or several mantle plumes. Exceptions are the western southeast Indian ridge (area 9), where the trailing flank is fast, in accordance with Stein's *et al.*'s¹⁶ model, and the southwest Indian ridge (area 8), which is very complex, and has experienced severe changes in spreading direction. PAC, South Pacific; SSAT, southern South Atlantic; CSAT, central South Atlantic; NSAT, northern South Atlantic; NATL, North Atlantic; CATL, central North Atlantic; LABR, Labrador Sea; NGSE, Norwegian Greenland Sea; ESEI, eastern southeast Indian ridge; WSEI, western southeast Indian ridge; SWIN, southwest Indian ridge; CIND, central Indian ridge.

main hotspots⁸ (Fig. 1). Hotspots may cause ridge jumps by pressure-release melting of material flowing towards the ridge, causing excess dyke intrusion on the ridge flank proximal to the hotspot. The buoyancy of the plume material increases the spreading force, which depends on the buoyancy times its depth^{13,18}. Deep plume buoyancy of sufficient magnitude can cause the point of maximum tension to be located off-axis, close to the plume.

A clear example of such 'trapping' of a ridge by a hotspot is seen in the South Atlantic (area 6). Here successive ridge jumps towards the Tristan da Cunha hotspot just east of the ridge caused consistent excess accretion on the South American plate (Fig. 1b). The absence of hotspots close to the mid-ocean ridge since initiation of spreading explains why spreading asymmetry is negligible in the Labrador Sea, in most of the North Atlantic and in the southeast Indian Ocean (area 11). In contrast, deficits in crustal accretion are found on those ridge flanks that are underlain by hotspots in the Norwegian-Greenland Sea, the South Atlantic and in the southwest and central Indian oceans. The current locus of active volcanism on Iceland is located on eastern Iceland²¹, indicating recent ridge jumps to the east, whereas earlier jumps were dominantly to the west (Fig. 1a). This supports models of a stationary Iceland hotspot²² with a vertical cylindrical structure²³ rather than a laterally moving plume over which the ridge has migrated from west to east. In the South Atlantic, the St Helena, Tristan da Cunha, Discovery, Shona and Bouvet hotspots are all located on the African plate, and have caused both large-scale ridge propagation events as well as successive jumps of the ridge axis towards Africa, leaving excess crust on South America. The same relationship of net asymmetries with hotspots on the slowly spreading ridge flank are found for spreading between Africa and India (area 10), showing a deficit in accretion on the African plate during the past 33 Myr, when Réunion was located underneath the African plate, and a deficit on the Indian plate before 33 Myr ago when the hotspot was situated east of the ridge (see also ref. 12). Kerguelen appears to have channelled asthenospheric material towards the southeast Indian ridge^{19,20}, resulting in crustal deficits in the corridors proximal to the hotspot on Antarctica (Fig. 1c), even though the plume is located $\sim 1,000 \text{ km}$ away from the ridge (see also ref. 12). The most extreme asymmetries observed, on the East Pacific Rise, are expressed as deficits in crustal accretion on the French Polynesian part of the Pacific plate, which is underlain by a thermal²⁴ or dynamically supported²⁵ "superswell" and numerous hotspots (Fig. 1d), indicating that successive ridge propagators/jumps²⁶ may have been triggered by plume-ridge interaction.

Fig. 1a-d illustrates that spreading asymmetry is ubiquitous in all ocean basins, but its occurrence is not dependent on the presence of ridge propagators¹⁴ (Fig. 1). This indicates that discrete ridge jumps, such as those described by Weiland *et al.*³, play an important role in causing cumulative asymmetries in accretion. In the absence of medium-to-large hotspots which channel material towards the ridge, small-scale ridge jumps occur randomly, with little net accretion asymmetry through time. Ridge-hotspot interaction biases this process by causing successive ridge jumps towards the plume. We conclude that ridge-plume interaction is the main cause of spreading asymmetries, even for large ridge-plume distances. □

Received 8 May; accepted 4 August 1998.

- Stoddard, P. R. & Stein, S. A kinematic model of ridge-transform geometry evolution. *Mar. Geophys. Res.* **10**, 181-190 (1988).
- Cande, S. C., LaBrecque, J. L. & Haxby, W. F. A high resolution seafloor spreading history of the South Atlantic. *J. Geophys. Res.* **93**, 13479-13492 (1988).
- Weiland, C., Wilson, D. S. & MacDonald, K. High-resolution plate reconstruction of the southern Mid-Atlantic Ridge. *Mar. Geophys. Res.* **17**, 143-166 (1995).
- Hayes, D. E. Nature and implications of asymmetric seafloor spreading. *Geol. Soc. Am. Bull.* **87**, 994-1002 (1976).
- Sempéré, J.-C. *et al.* The Mid-Atlantic Ridge between 29°N and 31°30'N in the last 10 Ma. *Earth Planet. Sci. Lett.* **130**, 45-55 (1995).
- Kleinrock, M. C. & Humphreys, S. E. Structural asymmetry of the TAG rift valley: Evidence from a near-bottom survey for episodic spreading. *Geophys. Res. Lett.* **23**, 3439-3442 (1996).
- Müller, R. D., Roest, W. R., Royer, J.-Y., Gahagan, L. M. & Sclater, J. G. Digital isochrons of the world's ocean floor. *J. Geophys. Res.* **102**, 3211-3214 (1997).
- Müller, R. D., Royer, J.-Y. & Lawver, L. A. Revised plate motions relative to the hotspots from combined Atlantic and Indian Ocean hotspot tracks. *Geology* **21**, 275-278 (1993).

9. Müller, R. D., Royer, J.-Y. & Lawver, L. A. *A Review of Absolute Plate Motion Models from Jurassic to Present Day* (Tech. Rep. No. 112) (Institute for Geophysics, Univ. Texas, Austin, 1991).
10. Morgan, W. J. in *The Oceanic Lithosphere* (ed. Emiliani, C.) 443–487 (Wiley, New York, 1981).
11. Phipps-Morgan, J., Morgan, W. J., Zang, Y.-S. & Smith, W. H. F. Observational hints for a plume-fed, suboceanic asthenosphere and its role in mantle convection. *J. Geophys. Res.* **100**, 12753–12767 (1995).
12. Schilling, J. G. Fluxes and excess temperatures of mantle plumes inferred from their interaction with migrating mid-ocean ridges. *Nature* **352**, 397–403 (1991).
13. Sleep, N. H. Hotspots and mantle plumes: Some phenomenology. *J. Geophys. Res.* **95**, 6715–6736 (1990).
14. Small, C. Observations of ridge-hotspot interactions in the Southern Ocean. *J. Geophys. Res.* **100**, 17931–17946 (1995).
15. Rouzo, S., Rabinowicz, M. & Briais, A. Segmentation of mid-ocean ridges with an axial valley induced by small-scale mantle convection. *Nature* **359**, 795–798 (1995).
16. Stein, S., Melosh, H. J. & Minster, J. B. Ridge migration and asymmetric sea-floor spreading. *Earth Planet. Sci. Lett.* **36**, 51–62 (1977).
17. Sleep, N. H. Formation of oceanic crust: some thermal constraints. *J. Geophys. Res.* **80**, 4032–4042 (1975).
18. Fujita, K. & Sleep, N. H. Membrane stresses near mid-ocean ridge-transform intersections. *Tectonophysics* **50**, 207–221 (1978).
19. Phipps-Morgan, J. & Smith, W. H. F. Flattening of the sea-floor depth-age curve as a response to asthenospheric flow. *Nature* **359**, 524–527 (1992).
20. Grevemeyer, I. Hotspot-ridge interaction in the Indian Ocean: constraints from Geosat/ERM altimetry. *Geophys. J. Int.* **126**, 796–804 (1996).
21. Oskarsson, N., Steinthorsson, S. & Sigvaldason, G. E. Iceland geochemical anomaly: origin, volcanotectonics, chemical fractionation and isotope evolution of the crust. *J. Geophys. Res.* **90**, 10011–10025 (1985).
22. Lawver, L. A. & Müller, R. D. Iceland hotspot track. *Geology* **22**, 311–314 (1994).
23. Wolfe, C. J., Bjarnason, I. T., VanDecar, J. C. & Solomon, S. Seismic structure of the Iceland mantle plume. *Nature* **385**, 245–247 (1997).
24. McNutt, M. K. & Judge, A. V. The superswell and mantle dynamics beneath the South Pacific. *Science* **248**, 933–1048 (1990).
25. Stein, C. A. & Stein, S. in *The Mesozoic Pacific: Geology, Tectonics, and Volcanism* (eds Pringle, M. S., Sager, W. W., Sliter, W. V. & Stein, S.) 53–76 (Am. Geophys. Union, Washington DC, 1993).
26. Goff, J. A. & Cochran, J. R. The Bauer scarp ridge jump: A complex tectonic sequence revealed in satellite altimetry. *Earth Planet. Sci. Lett.* **141**, 21–33 (1996).
27. Sandwell, D. T. & Smith, W. H. F. Marine gravity anomaly from ERS-1, Geosat and satellite altimetry. *J. Geophys. Res.* **102**, 10039–10045 (1997).
28. Munsch, M., Antoine, C. & Gachon, A. Evolution tectonique de la région Tuamotu, océan Pacifique central. *C.R. Acad. Sci. Paris Ser. IIa* **323**, 941–948 (1996).
29. Müller, R. D., Royer, J.-Y. & Lawver, L. A. Revised plate motions relative to the hotspots from combined Atlantic and Indian hotspot tracks: reply. *Geology* **22**, 277–278 (1994).

Acknowledgements. We thank N. Sleep and S. Stein for comments on the manuscript, and R. Buick and A. Dutkiewicz for discussions.

Correspondence and requests for materials should be addressed to R.D.M. (e-mail: dietmar@es.su.oz.au).

Implications of *Deltatheridium* specimens for early marsupial history

Guillermo W. Rougier^{†*}, John R. Wible^{‡*} & Michael J. Novacek[†]

* Department of Anatomical Sciences and Neurobiology, School of Medicine, University of Louisville, Louisville, Kentucky 40292, USA

† Department of Vertebrate Paleontology, American Museum of Natural History, New York, New York 10024, USA

‡ Section of Mammals, Carnegie Museum of Natural History, Pittsburgh, Pennsylvania 15206, USA

We describe here two new specimens of the mammal *Deltatheridium pretrituberculare* from the Late Cretaceous period of Mongolia. These specimens provide information on tooth replacement in basal therian mammals and on lower jaw and basicranial morphology. Deltatheroidans, known previously from isolated teeth, partial rostra and jaws from the late Cretaceous of Asia^{1–4} and possibly North America^{5,6}, have been identified variously as eutherians^{1,7,8}, as basal metatherians (the stem-based clade formed by marsupials and their extinct relatives)^{3,9–11}, or as an outgroup to both eutherians and metatherians^{2,12–15}. Resolution of these conflicting hypotheses and understanding of the early evolution of the therian lineage have been hampered by a sparse fossil record for basal therians. The new evidence supports metatherian affinities for deltatheroidans and allows a comprehensive phylogenetic analysis of basal metatherians and marsupials. The presence of specialized marsupial patterns of tooth replacement and cranial

vascularization in *Deltatheridium* and the basal phylogenetic position of this taxon indicate that these features are characteristic of Metatheria as a whole. Other morphological transformations recognized here secure the previously elusive diagnosis of Metatheria^{3,14,15}. The new specimens of *Deltatheridium* illustrate the effectiveness of fairly complete fossil specimens in determining the nature of early evolutionary events.

Two specimens of *Deltatheridium pretrituberculare* were recovered from Ukhaa Tolgod, the Mongolian Late Cretaceous locality notable for the abundance and exquisite preservation of dinosaurs, lizards, birds and mammals¹⁶. The first specimen, PSS-MAE 133, is an adult represented by a partial skull, complete lower jaws and two ulnae. The second, PSS-MAE 132, is a juvenile, consisting of nearly complete jaws, disarticulated skull bones and several postcranial elements. Comparison of all known specimens of *Deltatheridium*^{1,2} indicate that there is a single species, *D. pretrituberculare*, with no subspecies (contra ref. 2).

The new specimens of *Deltatheridium* provide the following, revised dental formula: I4/3 C1/1 P3/3 M4/4. In contrast to previous observations^{1,2,8,13}, three lower incisors and four upper molars are present. I₂, the largest incisor, is 'staggered' as in several groups of metatherians¹⁷. I₂ and I₃ are spatulated, but the crown of I₁ is missing in all known specimens. Previous reports of either one or two incisors in *Deltatheridium* (the main feature distinguishing two reported subspecies²) are artefactual. A tiny fourth upper molar is present bilaterally in PSS-MAE 133 (Fig. 1); this tooth and its alveolus were missing or unrecognized in earlier specimens, which led to the incorrect count of three upper molars. The presence of only three molars is unusual among metatherians and was used as evidence against the possible marsupial affinities of *Deltatheridium*^{2,12,13}. M⁴ is positioned lingually to the metacone of M³, so it continues the lingual curvature and reduction of the posterior molar dentition present in deltatheroidans, *Holoclemensia* and *Potamotelses*¹⁸.

The skull of *Deltatheridium* also has derived features indicating marsupial affinity, including a premaxilla with a posteriorly directed process that reaches the alveolus of the canine (Fig. 1), a feature widely present in metatherians but absent in basal eutherians and Mesozoic outgroups. The lower jaw has a distinctive shelf-like, medially inflected angle (Fig. 2), a metatherian feature that is absent in Mesozoic outgroups, monotremes and eutherians¹⁹.

Study of the second specimen, PSS-MAE 132, indicates that the braincase morphology of *Deltatheridium* was similar to that of therian mammals in genera, with an extensive squama of the squamosal and an anterior lamina absent from the braincase wall, and of marsupials in particular, with a deep zygomatic process of the squamosal, also present in the Early Cretaceous prototribosphenidan *Vincelestes*. The petrosals (Fig. 3) are similar to those attributed to metatherians from the Late Cretaceous of North America²⁰, showing two major metatherian synapomorphies: first, an absence of vascular sulci on the promontorium, indicating a marked reduction or complete absence of the stapediaal arterial system; and second, a small, horizontally orientated prootic canal connected to the postglenoid venous system.

Perhaps the most distinctive similarity between *Deltatheridium* and living marsupials is the tooth-replacement pattern. Unlike any other group of mammals, marsupials replace only one tooth postnatally, the last premolar^{21–23}. The jaws of PSS-MAE 132 show several teeth in the process of eruption (Fig. 4). Although the first two premolars show substantial wear and are fully erupted, the canine and P₃ are erupting; the former is about halfway out and the posterior accessory cusp of the latter is at the level of the alveolar margin. M₃ has a fully functional trigonid, but the talonid is still at the level of the alveolar margin, whereas the smaller M₄ is lodged deep in a crypt and rotated about 50° from the horizontal axis and 35° from the mandibular axis. Regular X-rays, computerized-tomography scanning and dissection of the right jaw did not